Fabrication of nanoparticles and nanostructures using ultrafast laser ablation of silver with Bessel beams

2015 Laser Phys. Lett. 12 036003

(http://iopscience.iop.org/1612-202X/12/3/036003)

IOP Publishing | Astro Ltd Laser Physics Letters
Laser Phys. Lett. **12** (2015) 036003 (10pp) doi:10.1088/1612-2011/12/3/036003

Fabrication of nanoparticles and nanostructures using ultrafast laser ablation of silver with Bessel beams

G Krishna Podagatlapalli[1], Syed Hamad[2], Md Ahamad Mohiddon[3] and S Venugopal Rao[1]

[1] Advanced Center of Research in High Energy Materials (ACRHEM), University of Hyderabad, Prof. C. R. Rao Road, Hyderabad 500046, Telanagana, India
[2] School of Physics, University of Hyderabad, Prof. C. R. Rao Road, Hyderabad 500046, Telanagana, India
[3] Centre for Nanotechnology, University of Hyderabad, Prof. C. R. Rao Road, Hyderabad 500046, Telanagana, India

E-mail: svrsp@uohyd.ernet.in and soma_venu@uohyd.ac.in

Received 27 September 2014, revised 30 November 2014
Accepted for publication 22 January 2015
Published 13 February 2015

Abstract

Ablation of silver targets immersed in double distilled water (DDW)/acetone was performed with first order, non-diffracting Bessel beams generated by focusing ultrashort Gaussian pulses (~2 and ~40 fs) through an Axicon. The fabricated Ag dispersions were characterized by UV-visible absorption spectroscopy, transmission electron microscopy and the nanostructured Ag targets were characterized by field emission scanning electron microscopy. Ag colloids prepared with ~2 ps laser pulses at various input pulse energies of ~400, ~600, ~800 and ~1000 μJ demonstrated similar localized surface plasmon resonance (LSPR) peaks appearing near 407 nm. Analogous behavior was observed for Ag colloids prepared in acetone and ablated with ~40 fs pulses, wherein the LSPR peak was observed near 412 nm prepared with input energies of ~600, ~800 and ~1000 μJ. Observed parallels in LSPR peaks, average size of NPs, plasmon bandwidths are tentatively explained using cavitation bubble dynamics and simultaneous generation/fragmentation of NPs under the influence of Bessel beam. Fabricated Ag nanostructures in both the cases demonstrated strong enhancement factors (>10^6) in surface enhanced Raman scattering studies of the explosive molecule CL-20 (2,4,6,8,10,12-Hexanitro-2,4,6,8,10,12-hexaazaisowurtzitane) at 5 μM concentration.

Keywords: silver nanoparticles, silver nanostructures, picosecond, femtosecond, Bessel beam, SERS, CL-20

S Online supplementary data available from stacks.iop.org/LPL/12/036003/mmedia

(Some figures may appear in colour only in the online journal)

1. Introduction

Laser ablation of plasmonic metals in aqueous media is a prominent top down lithographic process which is environmental friendly for efficient fabrication of nanoparticles (NPs) and nanostructures (NSs) [1–10]. Inherent mechanisms of metal ablation by laser pulses and the effects of liquid media on metallic plume lead to a transient interaction at the metallic plume–liquid interface, which plays a crucial role in the effective dynamics of cavitation bubble (CB). The mechanisms are very complicated and there is no unified theory, to date, explaining the comprehensive temporal evolution of CB dynamics [11–15]. Laser ablation dynamics of metals in liquids simultaneously depend on laser parameters such as wavelength,

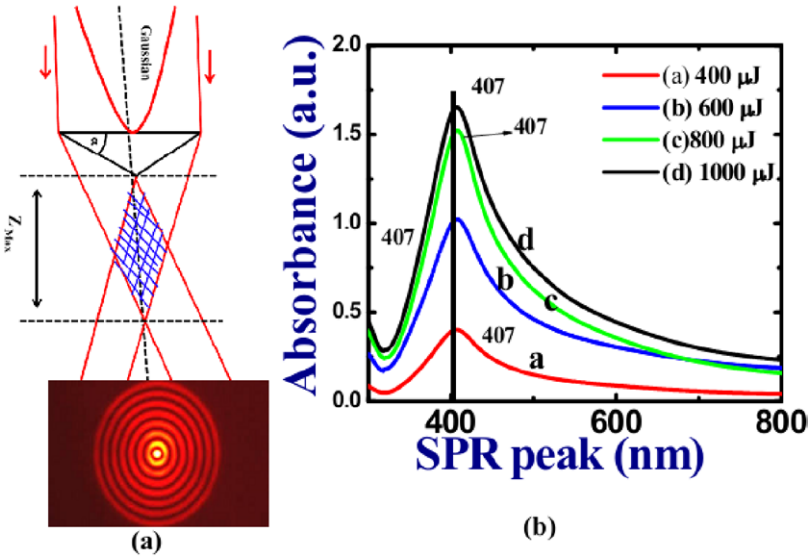

Figure 1. (*a*) Geometry of a focused Gaussian pulse using conical lens (Axicon) and formation of a Bessel beam pattern. (*b*) UV–vis absorption spectra of Ag colloids prepared in DDW; energies per pulse at which ablation was carried out is mentioned in the figure.

repetition rate, pulse duration, energy per pulse, and focusing geometry. Along with laser parameters, properties of the liquid medium (e.g. polarity, density, surface tension, viscosity) [2], roughness of the surface [4] also play an important role on ablation products. Most of the experiments in this field were carried out by laser pulses with focused Gaussian pulses and with conventional convex lenses. Surprisingly, the utility of non-diffracting beams in this field is not yet explored. In conventional Gaussian beam focusing experiments, efficient nanomaterials generation is possible when the spot size (beam waist) on the target is very small. However, the least beam waist minimizes the depth of focus (Z_{max}) which, in fact, introduces artifacts and creates a loss of control on the position of the beam waist for placing the sample exactly at focus. The focusing of Gaussian pulses through an Axicon (shown in figure 1(*a*)) eliminates the aforesaid problems by offering a considerable depth of focus. Additionally, it maintains comparatively similar spot size without any translational spread due to diffraction effects. Moreover, these non-diffracting Bessel beams exhibit nearly a constant intensity profile along their propagation [16, 17]. Salient features of Bessel beams such as self reconstruction and stability under nonlinear propagation make them extensively useful in extremely localized and controlled energy deposition in transparent materials. Matsuoka *et al* reported processing of metal targets with Bessel beams, but could not achieve efficient deep microstructures because of linear absorption in metals [18–20]. Our interest is to fabricate surface NSs and NPs and therefore we achieved this with Bessel beams for the first time, to the best of our knowledge. Futhermore, aberrations can be rendered insignificant in this case compared to the case of focusing by conventional convex lenses. Interference of conical wave front made by an Axicon is the primary reason to produce Bessel beam, which has the field and intensity distribution given by $E(\rho) = E_0 \exp(-\rho^2/\omega^2)$ where E_0 is the on-axis field amplitude, ρ is radial distance from the propagation axis Z, ω-radius of Gaussian beam. In this letter we present the results from the experiments where (a) we tried to exploit the uniqueness of non-diffracting Bessel beams over conventional Gaussian beams, (b) compared the performance of Ag NPs fabricated by picosecond (ps)/femtosecond (fs) laser pulses and provided possible mechanisms on the basis of CB for NPs with similar average sizes at different pulse energies, (c) studied the surface enhanced Raman activity of CL-20 (2,4,6,8,10,12-Hexanitro-2,4,6,8,10,12-hexaazaisowurtzitane) from Ag NSs fabricated with ~2 ps/~40 fs laser pulses.

2. Experimental details

Ultrafast laser ablation was performed by means of a chirped pulse amplified (CPA) Ti:sapphire laser system (LEGEND, Coherent) delivering nearly transform limited laser pulses (~2 ps/~40 fs, 1 kHz repetition rate) at a central maximum of 800 nm. Both ps and fs amplifiers were seeded by ~15 fs (full width at half maximum (FWHM) of ~55 nm) pulses from an oscillator (MICRA, Coherent, 1 W, 80 MHz, 800 nm central wavelength). Complete details of the experimental procedure of the ablation of metal targets in aqueous media were explained in our earlier works [2, 3]. Briefly, 1 mm thick Ag targets (purchased from Alfa Aeser, 99.9% purity) with a plain surface immersed in high performance liquid chromatography (HLPC) grade double distilled water (DDW)/acetone (Sigma Aldrich) were placed in a Pyrex cell mounted on a motorized nano-direct X–Y–Z stage. The typical thickness of the liquid layer on the target surface was ~6 mm. Ps/fs laser pulses were focused onto the Ag target immersed in DDW/acetone by an Axicon (base angle = 25°). The focal plane was adjusted on the target surface by observing the plasma with a cracking sound, as reported in [21, 22]. To match the focal plane exactly with the target surface, initially the focus was adjusted on the target in the absence of DDW/acetone. Later, depending on the thickness of the liquid layer, focal plane displacement (with respect to the focal plane in air) was estimated and corrected [23]. Ablation

of the Ag target in DDW was performed with ~2 ps laser pulses wherein the target was moved by X–Y stages (Newport) to draw periodic lines at a separation ~60 μm (total 120 lines). The speeds of the X, Y stages were 0.05 m s^{-1}, 0.5 m s^{-1}, respectively. Accelerations of X, Y stages were 0.05 m s^{-2}, 0.5 m s^{-2}. Input pulse energies utilized in the ps ablation case were ~400, ~600, ~800 and ~1000 μJ. Similarly, ablation of the Ag target in Acetone was carried out by ~40 fs laser pulses. In this case, the Ag target in the focal plane of the Bessel beam was moved by the NTS nano-direct stage in which the vertical stage (Z) was utilized to adjust the focal point on the target surface and the other two were utilized to draw periodic lines (each line length was 5 mm, total lines of 80) on Ag targets with separation 25 μm. In this fs ablation case, pulse energies of ~600, ~800 and ~1000 μJ were utilized. Speeds of the X- and Y-stages utilized in fs ablation were 100 μm s^{-1} and 500 μm s^{-1}, respectively. The separation between the two line structures was ~50 μm. Typical duration of each sample ablation was ~40 min. After completion of the ablation, targets were removed and cleaned properly. Similarly, colloidal solution was taken in air tightened vessels to prevent them from oxidation.

Fabricated Ag nanostructured portions were utilized as SERS active platforms to detect/identify high energy molecules CL-20. After a nominal cleaning of each laser-exposed portion of the Ag target, CL-20 dissolved in Acetonitrile (5 μM concentration; quantity 10 μl) was taken with a micro-pipette to form a monolayer on the laser-exposed portion to absorb the molecules efficiently to the NSs. This was because multi-layers of analyte on the laser-exposed portion kills the surface activity of the nanostructured target. Distance between the NS and analyte molecule must be close to 3–4 nm because evanescent fields produced by nanomaterials are distance dependent. Raman spectra were recorded with an excitation wavelength 532 nm.

3. Results and discussion

Ag colloids prepared in DDW with ~2 ps laser pulses had different degrees of gray coloration whereas in acetone and with ~40 fs laser pulses they exhibited contrasts of light-yellow coloration. Thus, prepared Ag colloids were characterized using a UV-vis absorption spectrometer and the corresponding spectra are shown in figure 1(*b*). The localized surface plasmon peak position (LSPR) for the Ag colloids prepared at energies of ~400, ~600, ~800 and ~1000 μJ was positioned at 407 nm, which is in contrast to the reports to date on ablation obtained using Gaussian laser pulses. Even though the absorbance of colloids (measure of yield) changed in accordance to input energy, LSPR peak position did not change. As Garcia *et al* [24] explained, LSPR peak position is the combined effect of all neighboring NPs covered under the diameter of the light beam path. Other morphological characterizations such as TEM, UV-vis absorption provide global information on average sizes of NPs. The LSPR peak possibly shifts due to the sizes of neighboring NPs. But in the present case it was different, demonstrating the possibility of fabricating NPs of similar average sizes even at four different input energies. Figure 2(*a*) illustrates transmission electron microscopic (TEM) images of Ag colloids prepared with energies of ~400 μJ and an average size of 11 ± 5 nm. Figure 2(*b*) demonstrates a TEM image of Ag colloids prepared at ~600 μJ energy with an average size of 12 ± 6 nm. Similarly, figure 2(*c*) depicts Ag colloids prepared at ~800 μJ possessing an average size of 13 ± 5 nm. Figure 2(*d*) demonstrates a TEM image of Ag colloids prepared at ~1000 μJ exhibiting an average size of 13 ± 5 nm. In each case, the maximum number of particles considered for measurement was >300. Analysis of the TEM images revealed that the average sizes were ~12 nm, which is in contrast to earlier reports with conventional ns/ps Gaussian pulse focusing (by convex lenses) where the average size of NPs decreased as the fluence increased. In the fs regime, earlier reports revealed that the average size increased as the fluence increased. But in our case a different trend was observed in the case of average sizes for both ps/fs ablation.

The observed results could be tentatively explained using the inherent characteristics of Bessel beam's focusing geometry. During the focusing, Axicon provides longer depth of focus (Z_{max}) with a sharp central intensity which is surrounded by concentric circles of comparatively lower intensity. In the laser ablation by Bessel beam, the ablation threshold can be calculated from the fluence provided by the central lobe of Bessel beam on the target surface. Theoretical peak fluence of the main lobe is expressed as [25]

$$F(\rho,\omega) = \frac{Q\beta}{\omega}\{[(F_1(\rho/\omega)+F_2(\rho/\omega))J_0(\rho\beta)]^2 + [(F_1(\rho/\omega)-F_2(\rho/\omega))J_1(\rho\beta)]^2\}, \quad (1)$$

where Q is the pulse energy in Joules, ω is in m and β is in m^{-1}. J_0 and J_1 are zeroth-order and first-order Bessel functions of first kind.

$$F_1(\rho/\omega) = \sqrt{z_0+\rho/\omega}\exp[-(z_0+\rho/\omega)^2], \quad (2)$$

$$F_2(\rho/\omega) = \sqrt{z_0-\rho/\omega}\exp[-(z_0+\rho/\omega)^2]H(z_0-\rho/\omega). \quad (3)$$

Substituting (2) and (3) in the fluence equation (1), the maximum peak fluence of the central lobe can be obtained as

$$F = \frac{2Q\beta}{\omega\sqrt{e}}, \qquad \beta = \frac{2\pi(n-1)\alpha}{\lambda}, \quad (4)$$

where n is the refractive index of the material of the Axicon, α is the base angle as shown in figure 1(a) (left). The diameter of the Bessel beam at focus was estimated to be ~1.4 μm. Theoretical peak fluences of the central lobe at focus in air, calculated from equation (4), were ~29, ~43, ~58 and ~72 J cm^{-2}. These peak fluences were obtained using the values of n as 1.5168 (refractive index of Axicon material), α-0.4363 (equivalent radians for 25°), λ-800 nm and ω as 3 mm (radius of input Gaussian beam) for input pulse energies of ~400 μJ, ~600 μJ, ~800 μJ and ~1000 μJ, respectively. Peak intensity on the target surface was estimated by the diameter of the central lobe [26] of the Bessel beam on the target. The

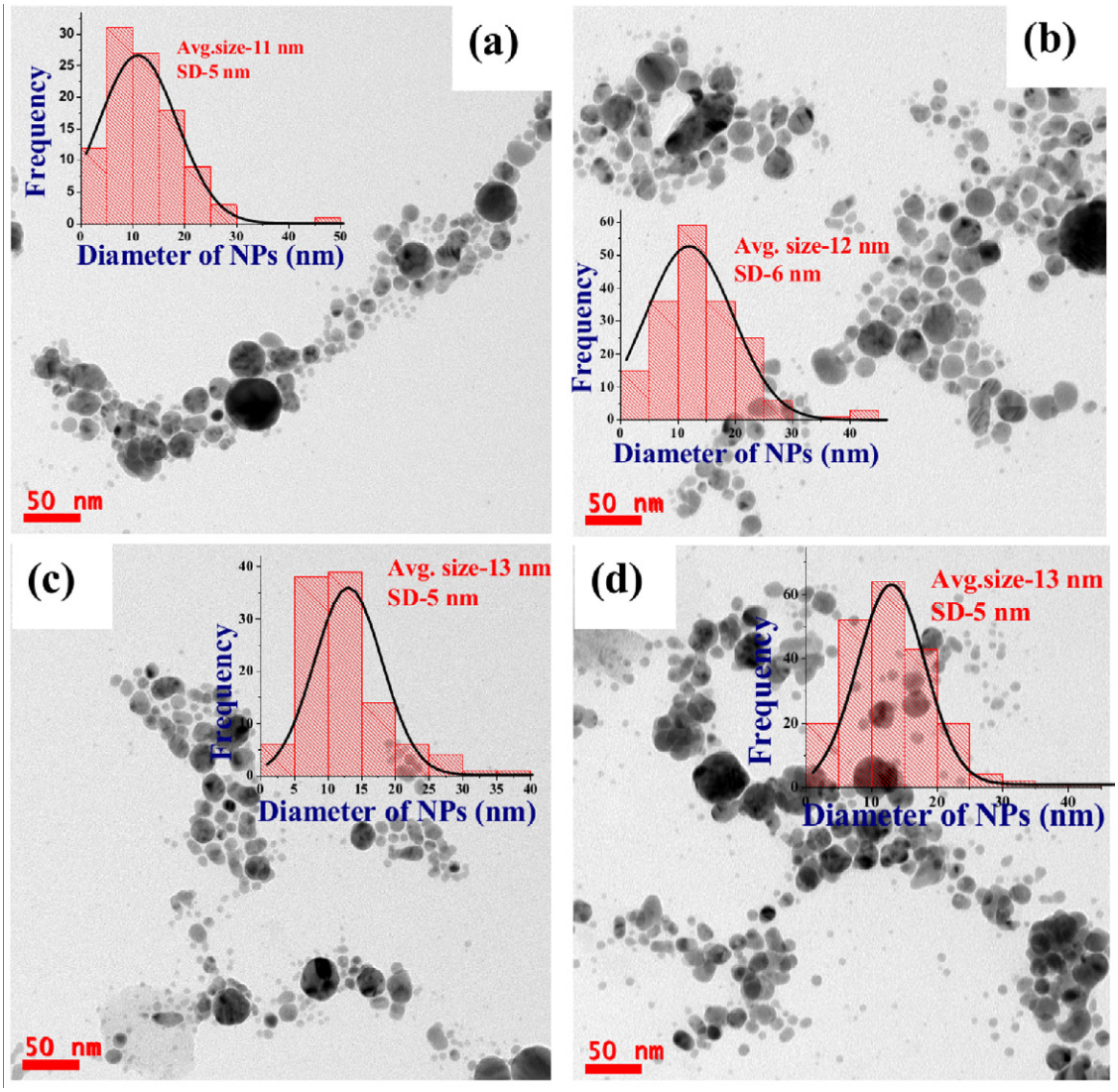

Figure 2. TEM images of Ag colloids prepared in DDW with ~2 ps laser pulses at pulse energies (*a*) 400, (*b*) 600, (*c*) 800 and (*d*) 1000 μJ. The inset of each figure depicts the yield distribution of Ag NPs.

estimated beam waist on the target surface was ~4.5 μm. In the Bessel beam ablation, ambiguity in the distribution of input energy over the entire transverse profile leads to erroneous results in the estimation of peak intensities. As a result, description of the obtained results on the basis of input pulse energy apparently seems appropriate compared to the peak intensity expressions. The percentage of energy distribution to the central lobe and the other rings is an important consideration in Bessel beam ablation to explain the possibilities of generation of white light continuum (WLC) and filament formations. This estimation was carried out by considering the central lobe energy measured with an aperture and a power meter (data is presented in the supporting information).

To confirm the observation of similar surface plasmon resonance (SPR) peak positions for Ag colloids prepared at different pulse energies, experiments were carried out on Ag targets with ~40 fs laser pulses in acetone. Typically each scan lasted for 30 min and the utilized pulse energies were ~600, ~800 and ~1000 μJ. These Ag colloids also exhibited similar behavior, evident from the UV-visible absorption spectra presented in figure 3(*a*). Evidently, the LSPR peak position was ~412 nm (~600 μJ), ~411 nm (~800 μJ) and ~412 nm (~1000 μJ). In this case the liquid media and pulse duration were different compared to the previous set of experiments but the trend observed was analogous. Even at different pulse energies, LSPR peak position did not change considerably and was stationed at 412 nm. Figures 3(*b*)–(*d*) depict the TEM images of Ag colloids in acetone prepared with non-diffracting Bessel beams (~40 fs) and the insets illustrate their size distribution. From the data analysis we recorded average sizes of 7 ± 1.5 nm, 7.5 ± 2.5 nm and 6.5 ± 1.5 nm, for Ag colloids prepared in acetone for ~600 μJ, ~800 μJ and ~1000 μJ input pulse energies, respectively.

Figure 4(*a*) demonstrates the variation in average sizes, SPR peak position, and figure 4(*b*) demonstrates absorbance, FWHM of the plasmon band with respect to the input energy in the case of ps ablation. Similarly, figure 4(*c*) demonstrates variation in average sizes, SPR peak position; figure 4(*d*) illustrates absorbance, FWHM of the plasmon band versus the input energy for the fs case. FWHM of the SPR band represents the possibility of sizes of the NPs and absorbance

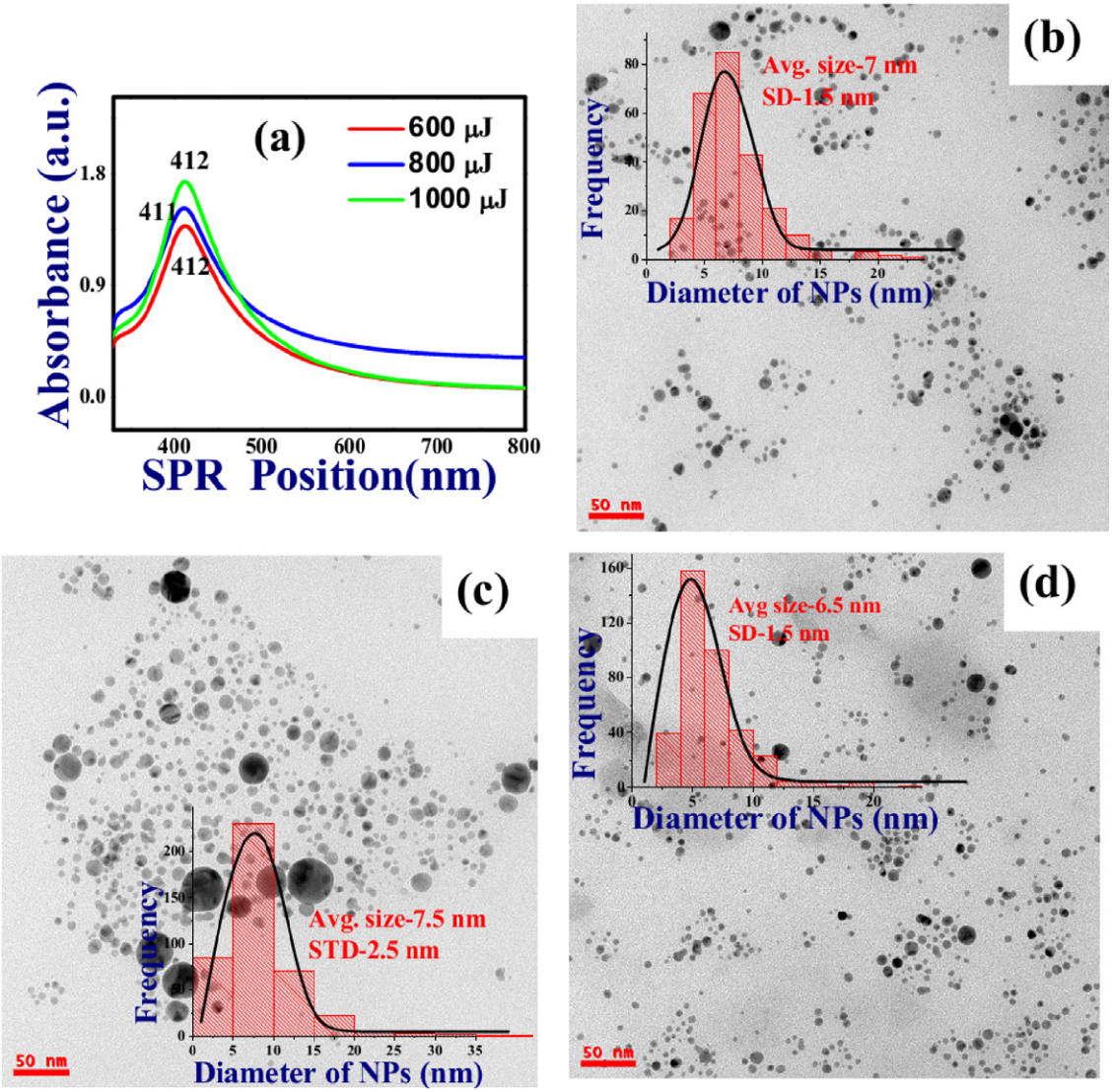

Figure 3. (*a*) UV–vis absorption spectra of Ag colloids prepared in acetone with ~40 fs laser pulses via Axicon focus. Corresponding TEM images of Ag colloids prepared at pulse energies (*b*) 600, (*c*) 800 and (*d*) 1000 μJ.

indicates the yield of NPs in the colloid. According to the data presented in figure 4, the average sizes were almost the same and absorbance had increased whereas plasmon band widths were similar for input energies of~400, ~600, ~800, ~1000 μJ (ps case). A similar trend was observed for the fs ablation case also (data shown in figures 4(*c*) and (*d*)). UV-vis absorption spectra provides global information, and therefore, we could conclude that average particle size was the same in ~2 ps ablation and ~40 fs ablations even at different pulse energies. These results are supported by the data obtained using TEM images. The complete dynamics of ablation must be investigated extensively to understand the interaction of the metal target with the Bessel beam field pattern underneath the liquid layer.

The results can, possibly, be understood using (a) CB dynamics on the target generated by the Bessel beam and (b) simultaneous fabrication of NPs by the central lobe and fragmentation by the field provided by the outer rings of the Bessel beam. Production of NPs in aqueous media using ultrashort pulses is a complex phenomenon and is yet to be understood completely. The process starts with absorption of the laser pulse by the target followed by electron–phonon relaxations, plasma formation, and generation of CB ending up with CB oscillations and collapse of the bubble. Following laser pulse absorption and in tens of ns, a shock wave can be generated from the target surface, expands in a few μs and finally starts oscillating, which results in a collapse in a duration of hundreds of μs. The dynamics of CB [27] is generally explained on the basis of a conventional Rayleigh–Plesset equation, but extension of this to laser ablation in which pressure inside the CB is inhomogeneous necessitates the equation to be modified accordingly [28]

$$R\frac{\mathrm{d}^2R}{\mathrm{d}t^2}+\frac{3}{2}\left(\frac{\mathrm{d}R}{\mathrm{d}t}\right)^2 = \frac{1}{\rho}\left(\left(p_0-p_v+\frac{2\sigma}{R_0}\right)\left(\frac{R_0}{R}\right)^{3\gamma}-p_0+p_v-\frac{2\sigma}{R_0}-\frac{4\eta}{R}\frac{\mathrm{d}R}{\mathrm{d}t}\right),$$

where R_0 is the CB radius at delay time 't' after the irradiation of the laser pulse, ρ is the density of liquid, p_0 is the hydrostatic pressure, p_v is the pressure inside the bubble, σ, η are the surface tension, viscosity of the liquid, γ is polytrophic

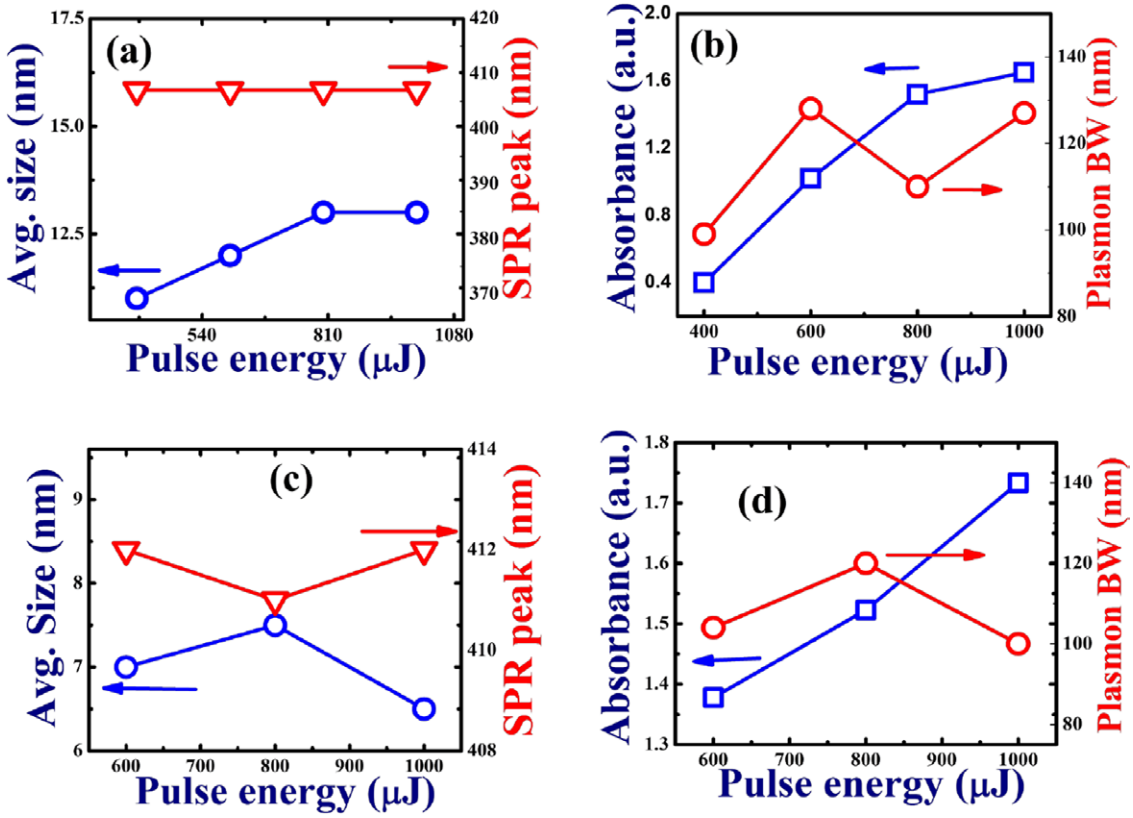

Figure 4. (*a*),(*b*) Average size of NPs, SPR peak position, absorbance, and plasmon band width of Ag NPs prepared with ~2 ps pulses in DDW, (*c*),(*d*) average size of NPs, SPR peak position, absorbance, and plasmon band width of Ag NPs prepared with ~40 fs pulses in acetone.

constant. On the right-hand side of the above equation, the pressure terms originate from various liquid parameters such as density, viscosity and surface tension. Moreover, p_v is the pressure due to the impact of the laser pulse which depends on the pulse energy. Since the Bessel beam field pattern is different, it probably resulted in a different amount of pressure at the laser/metal interface. These pressure terms influence the pressure developed inside the CB and, hence, maximum radius of the CB. Average sizes and size distribution of NPs produced are in general determined by the pressure and temperature inside the bubble and bubble oscillations. These pressures and temperatures depend on the incident field pattern and parameters of the liquid (density, surface tension, viscosity, refractive index). Herein, each study (for different pulse energies) was carried out in the same aqueous media (DDW and acetone) and hence the CB possibly could have been influenced by the Bessel beam field pattern. We strongly believe that the formation, oscillations, and collapse of the CB in this case are different to the conventional focusing case. However, to the best of our knowledge, there are no reports on the detailed cavitation dynamics with fs ablation in liquids, in general, and with Bessel beams, in particular. Furthermore, detailed theoretical modeling along with controlled experiments is necessary to exactly point out the mechanisms in fs Bessel beam ablation.

The geometric structure of Bessel beam suggests that all rings possibly have similar energies. Localization of central lobe intensity might cause local heating of the target surface to generate plasma proceeding towards formation of CB and its oscillations as discussed above. Meanwhile, surrounding rings possessing similar energies whose intensity is distributed over a wider area compared to the central lobe might not cause localized melting. But they could support cumulative nonlinear absorption of incident photons by the NPs produced by the central lobe. The mechanism of nonlinear absorption [29] in Ag NPs could be two-photon absorption (2PA) since the SPR peak of Ag NPs is in the vicinity of 400 nm with an extendable peak edge. Under the influence of a single pulse each NP approximately absorbs a few thousand photons which increase the internal energy of the NPs and, hence, generate heat through electron lattice collisions [30, 31]. When the heat reaches beyond boiling temperature, it forces them to fragment and subsequently disperses into the liquid medium. Consequently, consecutive fragmentation of NPs post fabrication could have resulted in the formation of a large number of NPs with relatively equal sizes as evident from UV–visible absorption spectra. This is due to the abrupt enhancement of the internal energy of NPs. Therefore, fragmentation continues inherently to fabricate NPs with the same average size. Increased fragmentation was confirmed from the absorbance and width of the plasmon band in both fs and ps cases. Furthermore, the surrounding dark regions/rings, which are due to destructive interference of conical wave fronts from the tip of Axicon, might act as potential wells and, probably, trap the generated NPs preventing aggregation. In addition to the above mentioned likelihood scenario for the observed results, the probability of WLC generation and multiple filamentation

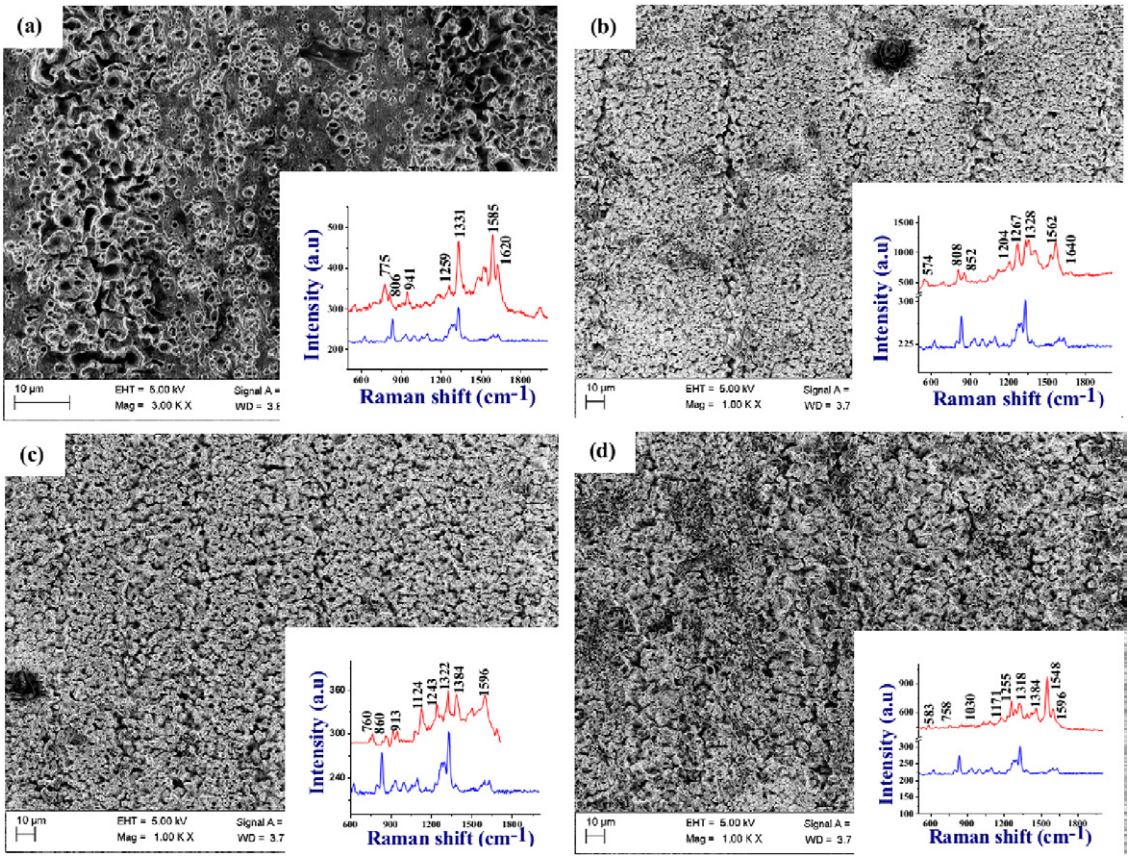

Figure 5. FESEM image Ag targets with Bessel beams at energies (*a*) 400, (*b*) 600, (*c*) 800, (*d*) 1000 μJ. Insets show the SERS spectra of CL-20 (5 μM, red/top curves) from the laser-exposed portions while the blue/bottom curves represent the 0.1 M CL-20 Raman spectra obtained from silicon wafer. Time of integration was 0.5 s for all the cases.

was investigated in a systematic manner. As a part of this investigation, a visible plasma plume formed during the Ag ablation (in air and on stable and moving Ag targets in acetone) was recorded with a USB 4000 (Ocean Optics) spectrometer. WLC generation and the possibility of multiple filamentation with Bessel beams was also investigated [32–36]. Surface morphologies of laser-exposed Ag portions in air and acetone under the same experimental conditions were investigated. A detailed analysis of the results obtained from this study revealed the possibility of WLC contribution to the observed NPs and NSs to be minimal. Furthermore, SEM images of the Ag targets obtained after ablation in ambient air and acetone clearly indicated that multiple filamentation was not predominantly evident even though we observed some secondary structures (apart from the main craters due to the central lobe) probably resulting from the outer lobes of the Bessel beam used. Our WLC results obtained in this study are in agreement with earlier reports [32]. Complete details of this part of the study are summarized in the supporting information.

In addition to the characterizations of NPs, NSs were also utilized to investigate the surface activity via surface enhanced Raman scattering (SERS) studies of an explosive molecule CL-20 (2,4,6,8,10,12-Hexanitro-2,4,6,8,10,12-hexaazaisowurtzitane) at μM concentrations. Morphologies of the laser-exposed portions of Ag targets were characterized by field emission electron microscope (FESEM). FESEM images of Ag NSs fabricated with ~ 2 ps, ~40 fs laser pulses are shown in figures 5 and 6, respectively. The procedure for adsorption of the analyte molecules on the laser-exposed portion of the Ag targets is described in the experimental section. Under the influence of plasmonic field provided by the metal NSs, molecules adsorbed on the nanomaterial experience combined field due to incident photons and field due to the nanomaterial. This basic feature enables gigantic enhancements of the Raman signal in SERS [37–43] experiments. Insets of figures 5 and 6 demonstrate the FESEM images of laser-exposed Ag targets ablated with ~2 ps, ~40 fs pulses and corresponding SERS of CL-20 with mode assignments [44–46]. Assignments of the Raman active modes are provided in table 1. Enhancement factors (EFs) [47] for the seven Ag NS targets were obtained by comparing the SERS spectra with the normal Raman spectra of CL-20 recorded on a non-plasmonic (silicon) substrate.

$$\mathrm{EF} = \frac{I_{\mathrm{SERS}}}{I_{\mathrm{Raman}}}\frac{N_{\mathrm{Raman}}}{N_{\mathrm{SERS}}},$$

where

$$N_{\mathrm{SERS}} = \eta N_{\mathrm{A}} V C_{\mathrm{Sol}} \frac{A_{\mathrm{Laser}}}{A_{\mathrm{Substrate}}}, N_{\mathrm{R}} = N_{\mathrm{A}} V C_{\mathrm{Sol}} \frac{A_{\mathrm{Laser}}}{A_{\mathrm{Substrate}}}.$$

$I_{\mathrm{SERS}}/I_{\mathrm{R}}$ can be calculated from the area under the signature peak of the particular mode of interest. N_{SERS}—number of molecules from the laser machined Ag substrate giving rise

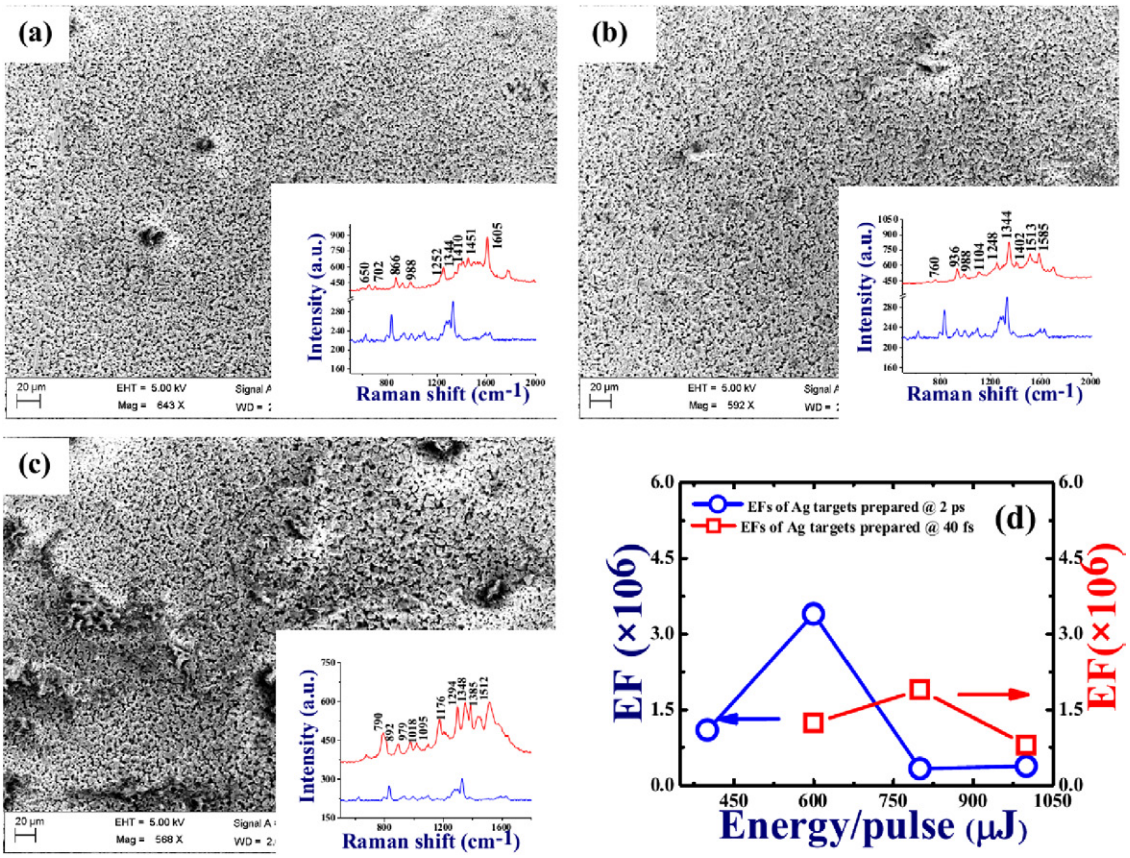

Figure 6. FESEM image Ag targets with Bessel beams prepared with ~40 fs laser pulses at energies (*a*) 600, (*b*) 600, (*c*) 800 μJ. Insets show the SERS spectra of CL-20 (5 μM, red/top curves) from the laser-exposed portions while the blue/bottom curves represent the 0.1 M CL-20 Raman spectra obtained from silicon wafer. (*d*) Comparison of enhancement factors for the Ag targets prepared with Bessel beams with ~2 ps and ~40 fs pulses. Time of integration was 0.5 s for all the cases.

Table 1. Observed active Raman modes of CL-20 adsorbed on Ag substrates ablated with Bessel beams using ~2 ps, ~40 fs laser pulses. Time of integration was 0.5 s for all measurements.

S. No	SERS shifts (0.1 M) (cm^{-1})	Assignments	Shifts in ps targets (cm^{-1})	Shifts in fs targets (cm^{-1})
1.	624	Ring deformation	—	650
2.	794	—	758, 760, 775	760, 790
3.	830	ONO bend, NO bend	806, 808, 852, 860	866, 892
4.	931	Ring stretch, NN stretch	913, 941	936
5.	995	Ring stretch, NN stretch	978	979, 988
6.	1050	Ring stretch, NN stretch	1030	1018
7.	1094	Ring stretch, NN stretch	1110	1095, 1104
8.	1158	CH bend, NO symmetric stretch	1124, 1171	1176
9.	1276	CH bend, NO symmetric stretch	1243, 1255, 1259,1267	1248, 1252
10.	1330	CH bend, NO symmetric stretch	1318, 1322, 1329, 1344	1344, 1348
11.	1376	CH bend, NO symmetric stretch	1354, 1384	1385, 1402, 1410
12.	1592	NO symmetric stretch	1548, 1562,	1512, 1513
13.	1629	NO stretch asymmetric	1596, 1620, 1640	1585, 1605

to a surface enhanced Raman signal, N_{Raman}—number of molecules giving rise to a Raman signal from the non-SERS surface, N_{A}—Avogadro number, V—total volume of the solution added onto the substrate, A_{Laser}—area of the laser spot, $A_{\text{Substrate}}$—total area of the substrate, η—adsorption factor. The adsorption factor was estimated using the procedure given in our earlier reports [7]. Each inset in figures 5 and 6 comprises the SERS spectrum from Ag NS (red, top curve) and normal Raman from silicon (blue, bottom curve).

As the data suggests, the highly elevated mode in CL-20 was 1330 cm^{-1} (CH bend + NO symmetric stretch) and the enhancement factors were estimated by considering I_{SERS} and I_{Raman} of the mode mentioned from NSs as well as the silicon target. Estimated enhancement factors were ~1.1 × 10^6,

~3.4 × 10^6, ~3.3 × 10^5, and ~3.8 × 10^5, for nanostructured targets prepared with ~2 ps pulses at ~400 μJ, ~600 μJ, ~800 μJ and ~1000 μJ, respectively. Similarly, enhancement factors for femtosecond targets are estimated as ~1.2 × 10^6, ~1.9 × 10^6 and ~8.0 × 10^5. To estimate these factors, the beam waist of the excitation wavelength (532 nm) at the focus was considered to be ~650 nm. Comparison of EFs is shown in figure 6(*d*) and found that in both regimes the order of magnitude of EFs were the same (~10^6). Further detailed theoretical and experimental studies are required to explain the complete ablation dynamics of metals in liquid media using non-diffracting Bessel beams.

4. Conclusions

Ablation with Bessel beams generated by focusing a Gaussian pulse (~2 ps and ~40 fs) through an Axicon was carried out for the first time, to the best of our knowledge, to fabricate NPs and NSs. Our experiments demonstrate the advantage over the conventional Gaussian focusing and difficulties arise in positioning the sample exactly at the focal plane. Our study also revealed that fabrication of well size controlled NPs are possible with Bessel beam ablation using Axicon. The results of ps ablation in DDW corroborated with the fs ablation studies in acetone since a similar trend was observed in the latter case too. The observed results have been tentatively understood using the special features of Bessel beams and CB dynamics followed by the central lobe self-healing. Simultaneous fragmentation could be possible along with fabrication when ablation is carried out with Bessel beams providing NPs of the same average sizes. The possibility of WLC generation and filamentation affecting the ablakon has been investigated and the results suggest the effects to be negligible. Fabricated NSs were utilized to examine the surface activity of laser-exposed portions through the SERS technique for a high performance explosive molecule CL-20 ((2,4,6,8,10,12-Hexanitro-2,4,6,8,10,12-hexaazaisowurtzitane) of 5 μM concentration and obtained enhancement factors of ~10^5. Our studies also revealed that targets prepared with ~2 ps laser pulses demonstrated slightly superior enhancements compared to fs targets.

Acknowledgments

Authors acknowledge DRDO for their continuous financial support. GKP acknowledges Mr Geo Philipp M, Dr Nirmal Viswanathan, School of Physics for providing the Axicon.

References

[1] Amendola V and Meneghetti M 2009 *Phys. Chem. Chem. Phys.* **11** 3805
[2] Podagatlapalli G K, Hamad S, Sreedhar S, Tewari S P and Venugopal Rao S 2012 *Chem. Phys. Lett.* **530** 93
[3] Podagatlapalli G K, Hamad S, Tewari S P, Sreedhar S, Prasad M D and Venugopal Rao S 2013 *J. Appl. Phys.* **113** 073106
[4] Podagatlapalli G K, Hamad S, Mohiddon M A and Venugopal Rao S 2014 *Appl. Surf. Sci.* **303** 217
[5] Hamad S, Podagatlapalli G K, Tewari S P and Venugopal Rao S 2013 *J. Phys. D. Appl. Phys.* **46** 485501
[6] Hamad S, Podagatlapalli G K, Vendamani V S, Nageswara S V S Rao, Pathak A P and Venugopal Rao S 2014 *J. Phys. Chem.* C **118** 7139
[7] Hamad S, Podagatlapalli G K, Mohiddon M A and Venugopal Rao S 2014 *Appl. Phys. Lett.* **104** 263104
[8] Hamad S, Podagatlapalli G K, Mohiddon M A, Venugopal Rao S 2015 *Chem. Phys. Lett.* **621** 171
[9] Desarkar H S, Kumbhakar P and Mitra A K 2013 *Laser Phys. Lett.* **10** 055903
[10] Mortazavi S Z, Parvin P and Reyhani A 2012 *Laser Phys. Lett.* **9** 547
[11] Kabashin A V and Meunier M 2003 *J. Appl. Phys.* **94** 7941
[12] Sylvestre J-P, Kabashin A V, Sacher E and Meunier M 2005 *Appl. Phys.* A **80** 753
[13] Sylvestre J P, Poulin S, Kabashin A V, Sacher E, Meunier M and Luong J H T 2004 *J. Phys. Chem.* B **108** 16864
[14] Boulais E, Lachaine R and Meunier M 2013 *J. Phys. Chem.* C **117** 9386
[15] Sylvestre J P, Kabashin A V, Sacher E, Meunier M and Luong J H T 2004 *J. Am. Chem. Soc.* **126** 7176
[16] Durnin J, Miceli J J and Eberly J H 1987 *Phys. Rev. Lett.* **58** 1499
[17] Courvoisier F, Zhang J, Bhuyan M K, Jacquot M and Dudley J M 2013 *Appl. Phys.* A **112** 29
[18] Garcés-Chávez V, McGloin D, Melville H, Sibbett W and Dholakia K 2002 *Nature* **419** 145
[19] Matsuoka Y, Kizuka Y and Inoue T 2006 *Appl. Phys.* A **84** 423
[20] Porras M A, Parola A, Faccio D, Dubietis A and Di Trapani P 2004 *Phys. Rev. Lett.* **93** 153902
[21] Nedderson J, Chumanov G and Cotton T M 1993 *Appl. Spectrosc.* **47** 1959
[22] Prochazka M, Stephanek J, Vicova B, Stephanek J, Vlckova B and Turpin P Y 1997 *Anal. Chem.* **69** 5103
[23] Manjon A M, Wagener P and Barcikowski S 2011 *J. Phys. Chem.* C **115** 5108
[24] Garcia M A 2011 *J. Phys. D: Appl. Phys.* **44** 283001
[25] Wu P, Sui C and Huang W 2014 *Photon. Res.* **2** 82
[26] Yalizay B, Ersoy T, Soylu B and Akturk S 2012 *Appl. Phys. Lett.* **100** 031104
[27] Wagener P, Ibrahimkutty S, Menzel A, Plech A and Barcikowski S 2013 *Phys. Chem. Chem. Phys.* **15** 3068
[28] De Bonis A, Sansone M, D'Alessio L, Galasso A, Santagata A and Teghil R 2013 *J. Phys. D: Appl. Phys.* **46** 445301
[29] Mafune F, Kohno J, Takeda Y and Kondow T 2002 *J. Phys. Chem.* B **106** 7574
[30] Takami A, Kurita H and Koda S 1999 *J. Phys. Chem.* B **103** 1226
[31] Mafune F, Kohno J, Takeda Y and Kondow T 2001 *J. Phys. Chem.* B **105** 9050
[32] Dota K, Pathak A, Dharmadhikari J A, Mathur D and Dharmadhikari A K 2012 *Phys. Rev.* A **86** 023808
[33] Duocastella M and Arnold C B 2012 *Laser Photon. Rev.* **6** 607
[34] Faccio D, Rubino E, Lotti A, Couairon A, Dubietis A, Tamŏsauskas G, Papazoglou D G and Tzortzakis S 2012 *Phys. Rev.* A **85** 033829
[35] Bhuyan M K, Courvoisier F, Phing H S, Jedrkiewicz O, Recchia S, Di Trapani P and Dudley J M 2011 *Eur. Phys. J. Spec. Top.* **199** 101
[36] Polesana P, Faccio D, Di Trapani P, Dubietis A, Piskarskas A, Couairon A and Porras M 2005 *Opt. Express* **13** 6160
[37] Fleischman M, Hendra P J and McQuillan A 1974 *J. Chem. Phys. Lett.* **26** 163
[38] Jeanmaire D L and Duyne R P V 1977 *Annu. Rev. Phys. Chem.* **84** 1
[39] Moskovits M 1985 *Rev. Mod. Phys.* **57** 783
[40] Kniepp K 1990 *Exp. Tech. Phys.* **38** 3
[41] Nie S and Emory S R 1997 *Science* **275** 1102

[42] Kneipp K, Wang Y, Kniepp H, Perelman L T, Itzkan I, Dasari R R and Feld M 1997 *Phys. Rev. Lett*. **78** 1667
[43] Amendola V and Meneghetti M 2012 *Adv. Funct. Mater*. **22** 353
[44] Goede P, Latypov N V and Ostmark H 2004 *Prop. Explos. Pyrotech*. **29** 205
[45] Ghosh M, Venkatesan V, Sikder A K and Sikder N 2012 *Def. Sci. J*. **62** 390
[46] Sanchita S, Deepika C, Krishnappa K B, Kumar S, Asthana S N and Umapathy S 2014 *J. Phys. Chem.* A **118** 2904
[47] Le Ru E C and Etchegoin P G 2009 *J. Chem. Phys*. **130** 181101